Supporting Information

Forming chemisorbed single-molecule junctions through loss of stable carbocations

Jazmine Prana,[a] Luana Zagami,[a] Kelly Yan,[a] Daniel Hernangómez-Pérez,*[,b] María Camarasa-Gómez,*[,c] and Michael S. Inkpen*[,a]

[a] *Department of Chemistry, University of Southern California, Los Angeles, CA 90089, USA*
[b] *CIC nanoGUNE BRTA, Tolosa Hiribidea, 76, 20018 Donostia-San Sebastián, Spain*
[c] *Centro de Física de Materiales (CFM-MPC) CSIC-UPV/EHU, 20018 Donostia-San Sebastián, Spain*

E-mail: d.hernangomez@nanogune.eu, maria.camarasa@ehu.eus, inkpen@usc.edu

Contents

1. General Information

Synthesis and Characterization

Manipulations under a nitrogen atmosphere were carried out in oven-dried glassware using standard Schlenk line techniques. No special precautions were taken to exclude air or moisture during workup unless otherwise stated. Anhydrous dichloromethane (CH_2Cl_2) and tetrahydrofuran (THF) were obtained by sparging with nitrogen and drying using a two-column solvent purification system packed with alumina (Pure Process Technologies, Nashua, NH, USA). Deionized water (initially 18.2 MΩ) was generated using an Arium® Mini Plus UV ultrapure water system (Sartorius AG, Goettingen, Germany). Deuterated solvents were purchased from Cambridge Isotope Laboratories, Inc., Cambridge Isotope Laboratories, Tewksbury, MA USA. Flash chromatography was performed using a Pure C-850 FlashPrep automated chromatography system and FlashPure EcoFlex flash cartridges (silica, irregular 40-63 μm particle size, 55-75 Å pore size; BUCHI Corporation, New Castle, DE, USA), or by hand using Alfa Aesar silica gel 60 (215-400 mesh). **^{t}Bu**[1] was prepared using established literature procedures. Other reaction solvents (sparged with nitrogen prior to use, where relevant), chemical reagents, and analyte molecules were commercially available and used without further purification. Reaction yields are unoptimized.

^{1}H and ^{13}C{^{1}H} NMR spectra were recorded at room temperature on Varian VNMRS 500 (500 MHz), VNMRS 600 (600 MHz), or Mercury 400 (400 MHz) NMR spectrometers. ^{1}H NMR data recorded in $CDCl_3$ and CD_2Cl_2, is referenced to residual internal C*H*Cl_3 (δ 7.26) and C*H*DCl_2 (δ 5.32) solvent signals, respectively.[2] ^{13}C{^{1}H} NMR data recorded in $CDCl_3$ and CD_2Cl_2 is referenced to internal *C*DCl_3 (δ 77.16) and *C*D_2Cl_2 (δ 53.84), respectively.[2] Mass spectrometry analyses were performed on a JEOL JMS-T2000GC AccuTOF GC-Alpha mass spectrometer (EI), at the Mass Spectrometry Lab, University of Illinois Urbana-Champaign.

Scanning Tunneling Microscope-based Break Junction (STM-BJ)

These details are reproduced here from a previous report, with only minor changes, for convenience.[3] STM–BJ measurements were performed using custom-built setups that have been described previously,[4–6] operated in ambient atmosphere or inside of a customized OMNI-Lab 4-port glovebox (Vacuum Atmospheres Company, Hawthorne, CA, USA). Hardware was controlled and analyses were performed using custom software (written using IgorPro, Wavemetrics Inc.,

OR, USA). Experiments were conducted at room temperature under ambient conditions unless otherwise stated. Tip–substrate distances were controlled with sub-angstrom precision using a single-axis preloaded piezoelectric actuator (P-840.1, Physik Instrumente, MA, USA). Tunneling currents were measured using a DLPCA-200 variable gain low noise transimpedance current amplifier (FEMTO Messtechnik GmbH, Berlin, Germany). Applying a bias between the tip and substrate, conductance was measured as a function of tip–substrate displacement (at 40 kHz acquisition rate) as the tip was repeatedly pushed into the substrate to reach a conductance of >5 G_0 (where $G_0 = 2e^2/h$) and then retracted 5–10 nm (at 20 nm/s) to break the contact. The resulting conductance-distance traces were compiled into 1D conductance histograms (using 100 bins/decade along the conductance axis), or 2D conductance-distance histograms (using 100 bins/decade along the conductance axis and 1000 bins/nm along the displacement axis). Traces in 2D histograms were aligned such that displacement = 0 nm where $G = 0.5\ G_0$. Color scales inset in 2D histograms are in count/1000 traces. Most probable conductance values for molecules studied here were obtained through Gaussian fits to their corresponding conductance peaks in 1D histograms.

STM tips were prepared from freshly cut Au wire (Ø = 0.25 mm; 99.998%, Alfa Aesar, MA, USA or 99.999%, Beantown Chemical, NH, USA). Substrates were prepared from evaporation of 100-200 nm Au (99.9985%, Alfa Aesar, or 99.999%, Angstrom Engineering Inc., ON, Canada) at a rate of ~1 Å/s onto mechanically polished AFM/STM steel specimen discs (Ted Pella Inc., CA, USA) with a COVAP Physical Vapor Deposition System (Angstrom Engineering Inc.) used exclusively for metal evaporation. Gold substrates were UV-ozone cleaned (Probe and Surface Decontamination Standard System, Novascan Technologies, Inc., IA, USA) and used for measurements that same day. Measurements in propylene carbonate (PrC; Millipore-Sigma, anhydrous, 99.7%) were performed using STM tips coated with wax (Apiezon® Vacuum Sealing Wax W, M & I Materials Ltd, Manchester, UK) to leave only the apex area exposed; this serves to minimize background (non-tunneling) electrochemical currents.[7] For glovebox measurements, freshly cleaned substrates were brought through the ports by sparging rather than pump-fill cycles, to minimize possible contamination from the glovebox rotary vane vacuum pump (RV8, Edwards Vacuum, Burgess Hill, UK).

Glovebox STM-BJ experiments were typically started at single digit or sub-ppm H_2O and O_2 concentrations, as measured by internal glove atmosphere sensors. O_2 concentrations typically

increase to 5-20 ppm during an experiment, as estimated by sensor readings upon re-initiation of air circulation. To minimize noise during data acquisition, circulation of the glovebox atmosphere was suspended, circulation valves were closed to isolate the catalyst, the vacuum pump was switched off, and the glovebox gloves were tied down to provide additional atmospheric stabilization. STM studies at 100°C were conducted using a custom-built resistive heating stage described previously.[3]

Directly before starting a solution measurement, ≥1,000 traces were collected to check the electrode surfaces were free from contamination. Analytes were typically studied as solutions (0.1-1 mM) tetradecane (TD; Millipore-Sigma, >99%), squalane (SQ; Millipore-Sigma, 96%), 1-bromonaphthalene (BN; Millipore-Sigma, 97%), 1-chloronaphthalene (CN; Thermo Fisher Scientific, 85%, remainder 2-chloronaphthalene), PrC, or 1,2,4-trichlorobenzene (TCB; Millipore-Sigma, ≥99%). All solvents used in the glovebox were first sparged with nitrogen and dried over 3Å molecular sieves.[8] Molecular sieves were activated by heating for ≥3.5 h at 350°C in a muffle furnace (Thermolyne, Thermo Scientific, Asheville, NC, USA), and stored in a desiccator until use.

Computational Details

Density Functional Calculations Details

Our density functional theory (DFT) calculations were carried out using the FHI-aims package,[9] which implements the closed-shell Kohn-Sham DFT formalism. We employed the Perdew-Burke-Ernzerhof (PBE) non-empirical, generalized gradient approximation for the exchange-correlation functional.[10] Scalar relativistic effects were incorporated via the zeroth-order regular approximation (ZORA) to account for relativistic corrections to the kinetic energy.[11] FHI-aims utilizes an optimized all-electron numeric atom-centered basis set. In this work, we adopted the so-called "light" computational settings, which correspond approximately to double-zeta basis set quality. The ground-state calculations were converged according to stringent self-consistent field (SCF) criteria: a particle density difference below 10^{-5} electrons/Å^3 between consecutive iterations, a total energy change under 10^{-7} eV, a variation in the sum of Kohn-Sham eigenvalues below 10^{-4} eV, and a force convergence threshold of 10^{-4} eV/Å. All optimized geometries were obtained using the trust-radius-enhanced variant of the Broyden-Fletcher-Goldfarb-Shanno

(BFGS) algorithm,[9] as implemented in FHI-aims. Structures were considered fully relaxed when all components of the residual atomic forces fell below the threshold of 10^{-2} eV/Å.

Ab initio Quantum Transport Calculations Details

The geometries of the model molecular junctions were determined through a well-established two-step procedure. First, the atomic positions of the molecule and the electrode apex were optimized using the methods and convergence criteria described above. This optimization was performed using pyramidal gold clusters comprising up to 11 gold atoms per tip. In the second step, the optimized molecular and tip geometries were kept fixed while additional gold layers were incorporated into the outer planes of the previously optimized electrode tips. This ensured proper screening of excess charge and accurate level alignment for subsequent quantum transport calculations.

The energy-dependent electronic transmission functions were computed within the linear response regime using the non-equilibrium Green's function (NEGF) formalism, as implemented in the AITRANSS transport module.[12–14] Each junction electrode was modeled as a pyramidal face-centered cubic (FCC) cluster of 37 atoms, cut along the (111) direction with a nearest-neighbor distance of 2.88 Å. The electrode self-energies were approximated using an energy-independent (Markovian) local model, given by $\Sigma(\mathbf{r}, \mathbf{r}') = i\eta(\mathbf{r})\delta(\mathbf{r} - \mathbf{r}')$. The local absorption rate, $\eta(\mathbf{r})$, was fine-tuned to ensure that the electronic transmission remained stable under smooth, moderate variations in $\eta(\mathbf{r})$ and was considered nonzero only within the outermost layers of the finite cluster.

2. Synthetic Details

4,4'-Bis(tritylthio)-1,1'-biphenyl (**Tr**)

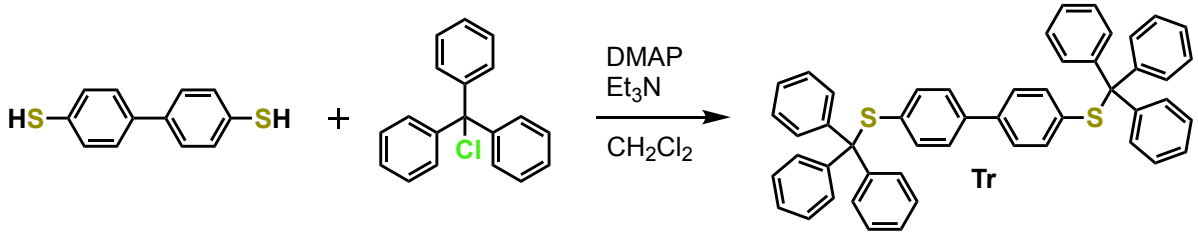

This compound was prepared using an adapted literature method.[15]

Biphenyl-4,4′-dithiol (0.192 g, 0.879 mmol) and then triethylamine (0.25 mL, 1.80 mmol) was added to a stirred solution of trityl chloride (0.630 g, 2.26 mmol) and 4-dimethylaminopyridine (0.036 g, 0.295 mmol) in CH_2Cl_2 (15 mL). The reaction flask was stoppered to minimize solvent evaporation. After 16 h, deionized water (~15 mL) was added to the green-yellow solution. The resulting mixture was extracted with CH_2Cl_2 (3 × ~20 mL), whereby the combined organic layers were dried over Na_2SO_4 and filtered before removing solvent by rotary evaporation. The crude product was preabsorbed onto Celite then purified using chromatography on a hexanes-packed SiO_2 column, eluting with 0:1→1:1 v/v CH_2Cl_2-hexanes. Isolated material was further recrystallized by slow removal of CH_2Cl_2 from a CH_2Cl_2/hexanes solution under vacuum to give **Tr** as a white crystalline solid (0.024 g, 4%). ^{1}H NMR (500 MHz, CD_2Cl_2): δ (ppm) 7.41 (d, J = 7.5 Hz, 12H, trityl-*H*), 7.22 (m, 18H, trityl-*H*), 7.14 (d, J = 8.6 Hz, 4H, biphenyl-*H*), 6.96 (d, J = 8.5 Hz, 4H, biphenyl-*H*). ^{13}C{^{1}H} NMR (126 MHz, CD_2Cl_2): δ (ppm) 144.91 (trityl Ph, C_{ispo}), 139.68 (biphenyl, CR_3), 135.05 (biphenyl, *C*-H), 134.21 (biphenyl, CR_3), 130.36 (trityl, *C*-H), 128.11 (trityl, *C*-H), 127.15 (trityl, *C*-H), 126.70 (biphenyl, *C*-H), 71.28 (trityl, CPh_3). HR-MS (EI+) m/z: 702.2396 ([M]$^+$ calc. for $C_{50}H_{38}S_2$: 702.2415).

4,4'-Bis(cyclohepta-2,4,6-trien-1-ylthio)-1,1'-biphenyl (**C_7H_7**)

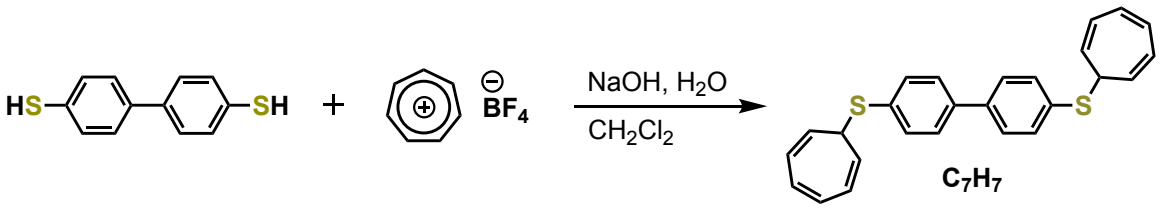

This compound was prepared using an adapted literature method.[16]

A nitrogen-sparged 0.1 M solution of NaOH in deionized water (2.6 mL, 0.26 mmol) was added to a stirred solution of biphenyl-4,4′-dithiol (0.103 g, 0.472 mmol) in CH_2Cl_2 (10 mL) under a N_2 atmosphere. Tropylium tetrafluoroborate (0.244 g, 1.37 mmol) was then added against a flow of N_2. After 19 h, the mixture was extracted into CH_2Cl_2 (~10 mL) then washed with brine (3 × ~25 mL). The organic layer was dried over Na_2SO_4 and filtered before removing solvent by rotary evaporation. The crude product was recrystallized by slow removal of CH_2Cl_2 from a CH_2Cl_2/hexanes solution under vacuum to give a yellow solid (0.049 g, 26%). ^{1}H NMR (400 MHz, CD_2Cl_2): δ (ppm) 7.49 (d, J = 7.2 Hz, 4H, biphenyl-*H*), 7.41 (d, J = 6.6 Hz, 4H, biphenyl-*H*), 6.64 (br s, 4H, C_7H_7-*H*), 6.29 (d, J = 9.3 Hz, 4H, C_7H_7-*H*), 5.58 (t, J = 8.4 Hz, 4H, C_7H_7-*H*), 3.99 (t, J = 6.8 Hz, 2H, C*H*-S).^{13}C{^{1}H} NMR (101 MHz, CD_2Cl_2): δ (ppm) 138.97 (biphenyl, *C*R$_3$), 135.30 (biphenyl, *C*R$_3$), 131.92 (C_7H_7, *C*-H), 131.56 (biphenyl, *C*-H), 127.52 (biphenyl, *C*-H), 127.38 (C_7H_7, *C*-H), 124.75 (C_7H_7, *C*-H), 46.10 (C_7H_7, *C*-S). HR-MS (EI+) m/z: 398.1168 ([M]$^+$ calc. for $C_{26}H_{22}S_2$: 398.1163).

4,4'-Bis(benzylthio)-1,1'-biphenyl (**Bn**)

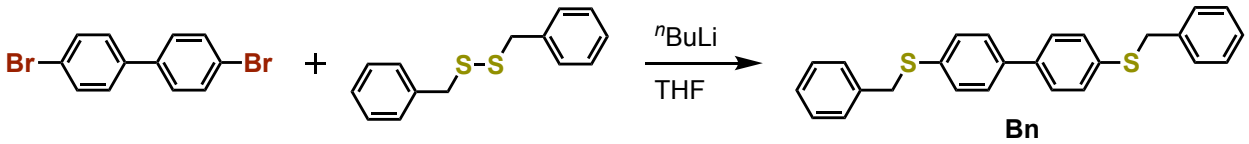

This compound was prepared using an adapted literature method.[17]

A solution of 1.6 M *n*-butyl lithium in hexanes (1.2 mL, 1.92 mmol) was added dropwise to a stirred solution of 4,4'-dibromobiphenyl (0.217 g, 0.696 mmol) in THF (6 mL) under a N_2 atmosphere at −78°C (dry ice/acetone bath). After 10 min, dibenzyl disulfide (0.681 g, 2.76 mmol) was added against a flow of N_2 and the mixture was allowed to warm to room temperature with stirring over 16 h. Deionized water (10 mL) was added to the resulting turbid orange solution to quench any unreacted organolithium species. The mixture was extracted into CH_2Cl_2 (10 mL), whereby the organic layer was washed with brine (3 × ~10 mL), dried over $MgSO_4$, and filtered before removing solvent by rotary evaporation. The crude product was preabsorbed onto Celite then purified using chromatography on a hexanes-packed SiO_2 column, eluting with hexanes. Isolated material was further recrystallized by slow removal of CH_2Cl_2 from a CH_2Cl_2/hexanes solution under vacuum to give **Bn** as a white crystalline solid (0.017 g, 6%). Spectroscopic data is consistent with previous reports.[17] ^{1}H NMR (500 MHz, CD_2Cl_2): δ (ppm) 7.48 (d, J = 8.5 Hz, 4H,

biphenyl-*H*), 7.35 (m, 8H, overlapping biphenyl-*H* and benzyl-*H*), 7.30 (m, 4H, benzyl-*H*), 7.24 (m, 2H, benzyl-*H*), 4.17 (s, 4H, C*H*$_2$). ^{13}C{^{1}H} NMR (126 MHz, CD_2Cl_2) δ (ppm) 138.52 (Ar, *C*R$_3$), 137.96 (Ar, *C*R$_3$), 136.18 (Ar, *C*R$_3$), 130.12 (Ar, *C*-H), 129.20 (Ar, *C*-H), 128.88 (Ar, *C*-H), 127.59 (benzyl, *C*-H), 127.49 (biphenyl, *C*-H), 39.00 (*C*H$_2$). HR-MS (EI+) m/z: 398.1167 ([M]$^+$ calc. for $C_{26}H_{22}S_2$: 398.1163).

(Cyclohepta-2,4,6-trien-1-ylthio)-phenyl (**PhC$_7$H$_7$**)

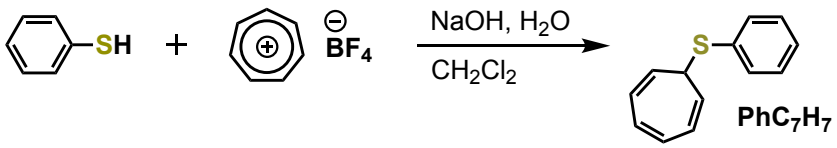

This compound was prepared using an adapted literature method.[16]

Thiophenol (0.2 mL, 1.9 mmol) was added to a stirred mixture of tropylium tetrafluoroborate (0.693 g, 3.89 mmol) in a nitrogen-sparged 0.1 M solution of NaOH in deionized water (7.1 mL, 0.71 mmol) under a N_2 atmosphere. After 20 h, the mixture was extracted into CH_2Cl_2 (~10 mL) then washed with 10% w/w sodium chloride in deionized water (3 × ~15 mL). The organic layer was dried over Na_2SO_4 and filtered before removing solvent by rotary evaporation. The crude product was preabsorbed onto Celite then purified using chromatography on a hexanes-packed SiO_2 column, eluting with hexanes. Solvent removal from selected fractions provided **PhC$_7$H$_7$** as a yellow oil (0.083 g, 21%). Spectroscopic data is consistent with previous reports.[16] ^{1}H NMR (600 MHz, $CDCl_3$): δ (ppm) 7.38 (d, *J* = 8.0 Hz, 2H, Ph-*H*), 7.27 (t, *J* = 7.5 Hz, 2H, Ph-*H*), 7.21 (t, *J* = 7.3 Hz, 1H, Ph-*H*), 6.64 (br s, 2H, C$_7$H$_7$-*H*), 6.27 (d, *J* = 10.6 Hz, 2H, C$_7$H$_7$-*H*), 5.56 (t, *J* = 8.2 Hz, 2H, C$_7$H$_7$-*H*), 3.91 (t, *J* = 6.8 Hz, 1H, C$_7$H$_7$-*H*). ^{13}C{^{1}H} NMR (151 MHz, $CDCl_3$): δ (ppm) 135.55 (Ph, *C*R$_3$), 131.68 (*C*-H), 131.20 (*C*-H), 128.95 (*C*-H), 126.99 (*C*-H), 126.84 (*C*-H), 124.70 (*C*-H), 45.92 (C$_7$H$_7$, *C*-S). HR-MS (EI+) m/z: 200.0655 ([M]$^+$ calc. for $C_{13}H_{12}S$: 200.0660).

3. Additional Conductance Data

Table S1. Conductance data from measurements of **^{t}Bu** in **Figures 2** and **3**.[a]

panel	geometry	conditions	V_{bias} (V)	conductance (G_0)	absolute area	P/C [b]
2a,3a	PP	TD	0.10	1.08×10^{-4}	0.745	0.54
	PC [c]		(first)	7.06×10^{-4} [c]	1.757 [c]	
	CC			4.23×10^{-3}	2.150	
3a	PP	TD	0.75	1.52×10^{-4}	0.887	0.82
	PC			1.01×10^{-3}	2.213	
	CC			5.46×10^{-3}	1.317	
3a	PP	TD	0.10	1.36×10^{-4}	0.711	0.52
	PC		(last)	9.17×10^{-4}	1.829	
	CC			5.51×10^{-3}	2.215	
2a,3b	PP	TD (N_2)	0.10	1.08×10^{-4}	1.201	1.17
	PC [c]		(first)	5.24×10^{-4} [c]	1.425 [c]	
	CC			3.23×10^{-3}	0.919	
3b	PP	TD (N_2)	0.75	1.46×10^{-4}	1.254	0.84
	PC			7.79×10^{-4}	2.164	
	CC			4.00×10^{-3}	1.686	
3b	PP	TD (N_2)	0.10	1.17×10^{-4}	1.471	1.06
	PC [c]		(last)	5.71×10^{-4} [c]	1.483 [c]	
	CC			3.44×10^{-3}	1.354	
2b	PP	SQ	0.10	1.11×10^{-4}	1.296	1.21
	PC [c]			5.00×10^{-4} [c]	1.838 [c]	
	CC			3.69×10^{-3}	0.908	
2b	PP	SQ (100°C)	0.10	1.19×10^{-4}	0.633	0.61
	PC			7.35×10^{-4}	1.645	
	CC			4.39×10^{-3}	1.544	
2c	PP	BN	0.10	1.25×10^{-4}	1.753	3.85
	PC			5.55×10^{-4}	1.187	
	CC			6.60×10^{-3}	0.016	
2c	PP	CN	0.10	1.13×10^{-4}	0.417	1.82
	PC			5.49×10^{-4}	0.525	
	CC			4.82×10^{-3}	0.111	
2d	PP	PrC	−0.10	9.47×10^{-5}	0.845	3.37
	PC			3.04×10^{-4}	0.519	
	CC			5.25×10^{-3}	0.068	

2d	PP	PrC	0.10	1.01×10^{-4}	1.160	4.16
	PC			3.00×10^{-4}	0.497	
	CC			6.40×10^{-3}	0.090	

[a] Measurements of **^{t}Bu** typically give three conductance peaks assigned to junctions with PP, PC, or CC geometries. Peak conductance values (G_{peak}), and areas, are obtained from Gaussian deconvolution of 1D histograms using MagicPlot (Magicplot Systems, LLC). [b] The ratio of physisorbed to chemisorbed contacts (P/C) is calculated using P/C = (areaPP + areaPC/2) / (areaCC + areaPC/2). [c] The width of the Gaussian fit to the PC feature was constrained (half-width at half-maximum = $10^{Gpeak \pm 0.45}$ G_0) to improve peak fits to PP and CC features.

Table S2. Conductance data from *repeated* measurements of **^{t}Bu** in **Figures S3** and **S4**.[a]

panel	geometry	conditions	V_{bias} (V)	conductance (G_0)	absolute area	P/C [b]
3b	PP	TD	0.10	1.19×10^{-4}	0.624	0.76
	PC [c]		(first)	7.69×10^{-4} [c]	1.627 [c]	
	CC			4.22×10^{-3}	1.082	
3b	PP	TD	0.75	1.46×10^{-4}	0.607	1.00
	PC			1.02×10^{-3}	2.394	
	CC			5.36×10^{-3}	0.604	
3b	PP	TD	0.10	1.10×10^{-4}	0.241	0.76
	PC		(last)	6.18×10^{-4}	0.932	
	CC			3.89×10^{-3}	0.464	
3c	PP	TD	0.10	1.22×10^{-4}	1.036	0.75
	PC			7.00×10^{-4}	2.015	
	CC			4.43×10^{-3}	1.728	
3c	PP	TD	0.75	1.39×10^{-4}	1.222	1.51
	PC [c]			7.10×10^{-4} [c]	2.196 [c]	
	CC			4.65×10^{-3}	0.442	
3e	PP	TD (N_2)	0.10	1.11×10^{-4}	1.006	0.93
	PC [c]			6.06×10^{-4} [c]	1.606 [c]	
	CC			3.31×10^{-3}	1.132	
3e	PP	TD (N_2)	0.75	1.48×10^{-4}	1.177	0.40
	PC [c]			9.46×10^{-4} [c]	3.094 [c]	
	CC			4.72×10^{-3}	5.197	
3h	PP	SQ	0.75	1.37×10^{-4}	1.249	1.16
	PC [c]			8.22×10^{-4} [c]	1.945 [c]	
	CC			4.65×10^{-3}	0.949	

3h	PP	SQ (100°C)	0.75	1.85×10^{-4}	0.448	0.46
	PC			1.15×10^{-3}	1.569	
	CC			5.37×10^{-3}	1.906	
4a	PP	BN (2)	0.10	1.56×10^{-4}	1.076	1.50
	PC			1.08×10^{-3}	2.128	
	CC			7.07×10^{-3}	0.346	
4b	PP	CN (2)	0.10	1.77×10^{-4}	0.665	2.99
	PC [c]			8.45×10^{-4} [c]	0.424 [c]	
	CC			4.44×10^{-3}	0.081	
4c	PP	PrC (2)	−0.10	1.06×10^{-4}	0.900	4.40
	PC			5.08×10^{-4}	0.298	
	CC			3.90×10^{-3}	0.090	
4c	PP	PrC (2)	0.10	9.73×10^{-5}	0.981	4.47
	PC			4.21×10^{-4}	0.416	
	CC			3.93×10^{-3}	0.058	

[a] Measurements of **^{t}Bu** typically give three conductance peaks assigned to junctions with PP, PC, or CC geometries. Peak conductance values (G_{peak}), and areas, are obtained from Gaussian deconvolution of 1D histograms using MagicPlot (Magicplot Systems, LLC). [b] The ratio of physisorbed to chemisorbed contacts (P/C) is calculated using P/C = (areaPP + areaPC/2) / (areaCC + areaPC/2). [c] The width of the Gaussian fit to the PC feature was constrained (half-width at half-maximum = $10^{Gpeak \pm 0.45}$ G_0) to improve peak fits to PP and CC features.

Table S3. Selected conductance data corresponding to **Figures 4**, **S8c**, and **S9**.[a]

entry	molecule	solvent	conductance (G_0)
1	**Tr**	TCB	5.29×10^{-3}
2	**C_7H_7**	TCB	1.13×10^{-2}
3a	**Bn**	TCB	8.00×10^{-4}
3b	**Bn**	TD	4.34×10^{-4}
4a	**H** [b]	TCB	5.46×10^{-3}
4b	**H** (2) [b]	TCB	4.10×10^{-3}
5	**Me** [b]	TCB	1.14×10^{-3}

[a] All data measured at V_{bias} = 0.1 V unless otherwise stated. Peak conductance values obtained from Gaussian fits to 1D histogram peaks. [b] Data reported in previous work.[1]

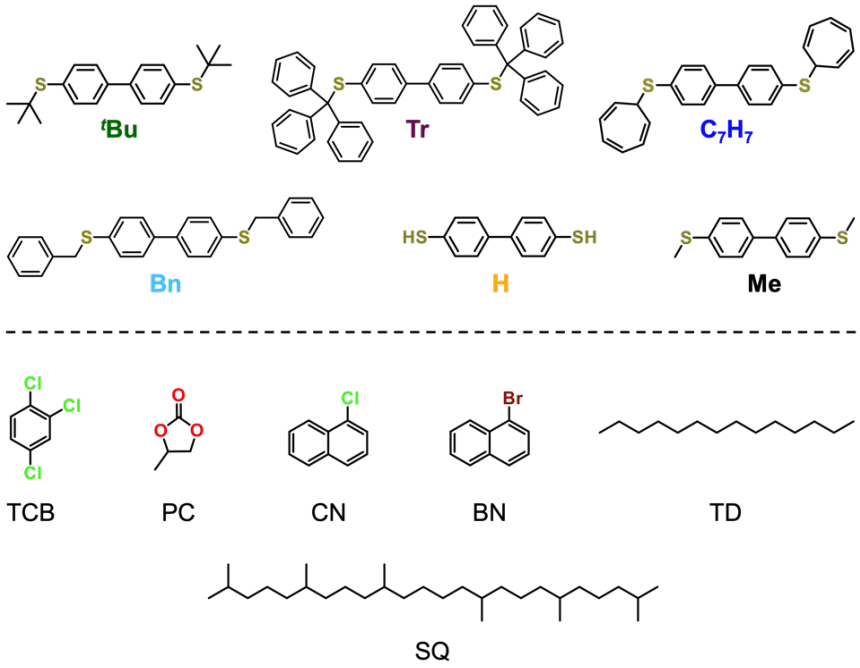

Figure S1. Molecular structures of all compounds (top) and solvents (bottom) used in this study.

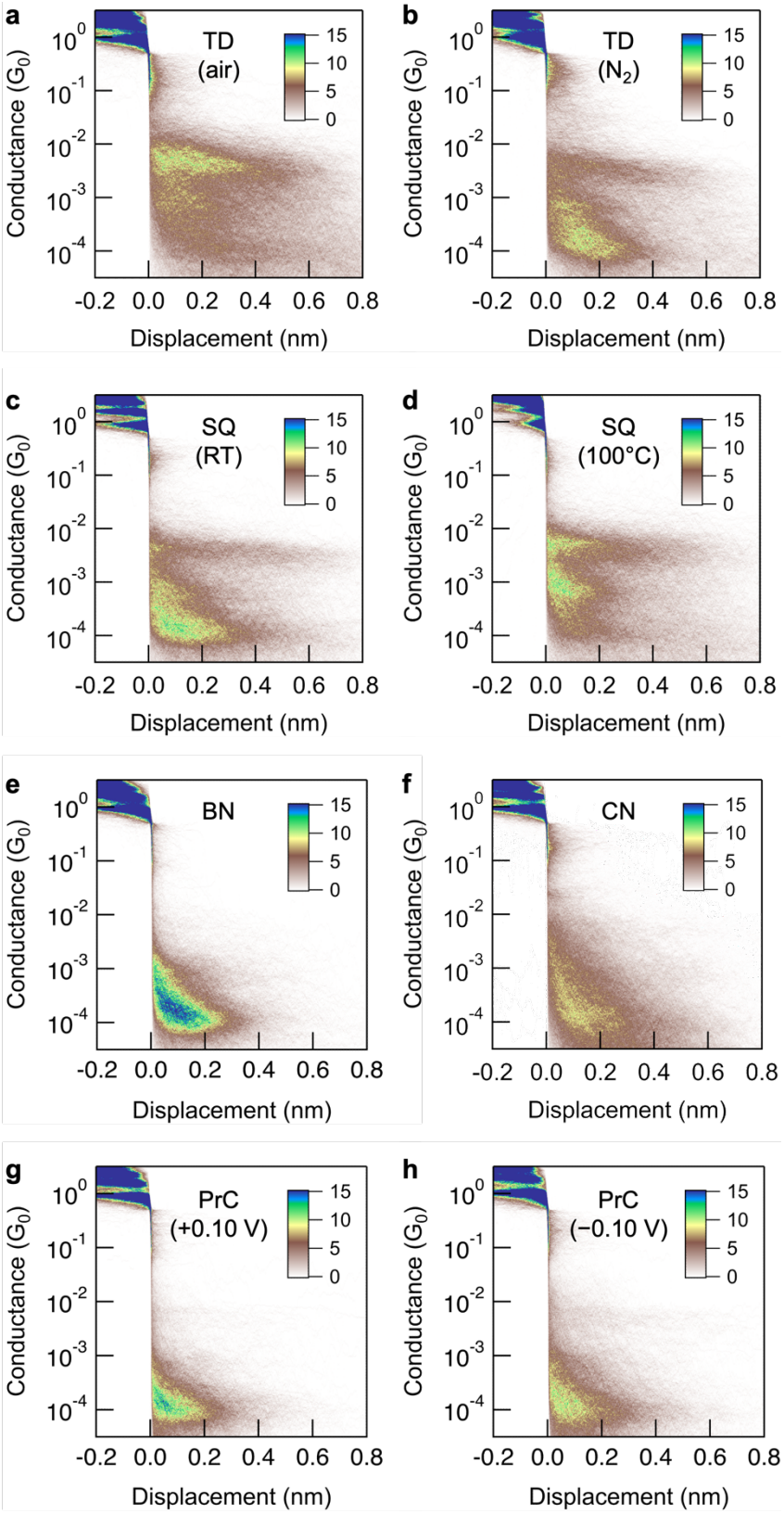

Figure S2. 2D conductance-displacement histograms obtained from measurements of ***t*Bu**, corresponding to the 1D conductance histograms shown in **Figure 2**.

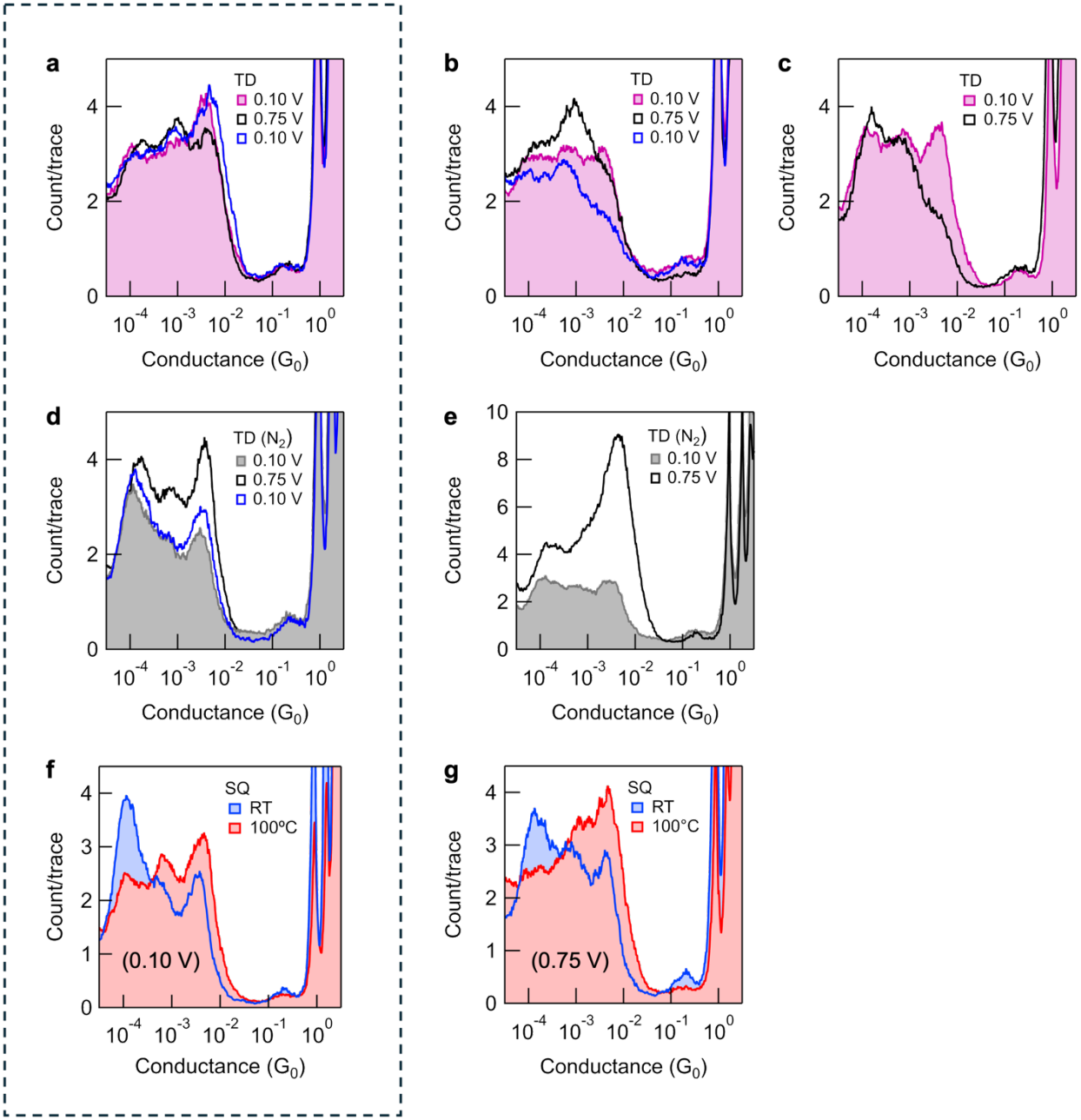

Figure S3. Overlaid 1D histograms for repeated measurements of **ᵗBu** performed in **(a-c)** TD in air at different V_{bias}, **(d-e)** TD under N_2 at different V_{bias}, **(f-g)** SQ in air at different V_{bias} and temperature. Boxed panels (a), (d), and (f) are reproduced here from **Figures 2b**, **3a**, and **3b**, for convenience. We clearly observe significant experiment variation between measurements. While no clear trends are observed with applied bias for TD measurements in air, data for TD measurements under N_2 show smaller P/C for larger V_{bias} (**Tables S2**, **S3**). A smaller P/C is also clearly observed for SQ measurements at 100°C relative to those performed at RT.

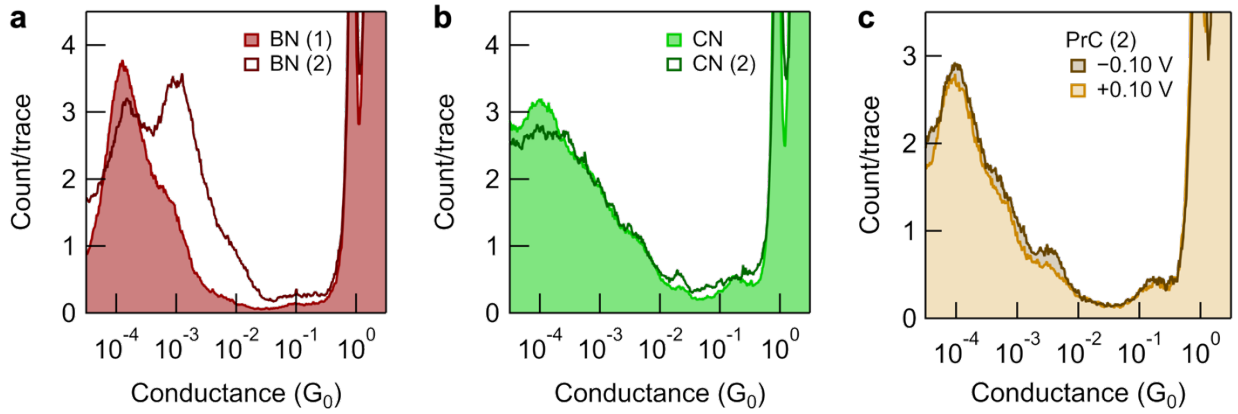

Figure S4. Overlaid 1D histograms for repeated measurements of **ᵗBu** performed in **(a)** BN and **(b)** CN at V_{bias} = 0.10 V, and **(c)** PC at V_{bias} = ±0.10 V. Solid histograms in panels (a) and (b) are reproduced here from **Figure 2c** for convenience.

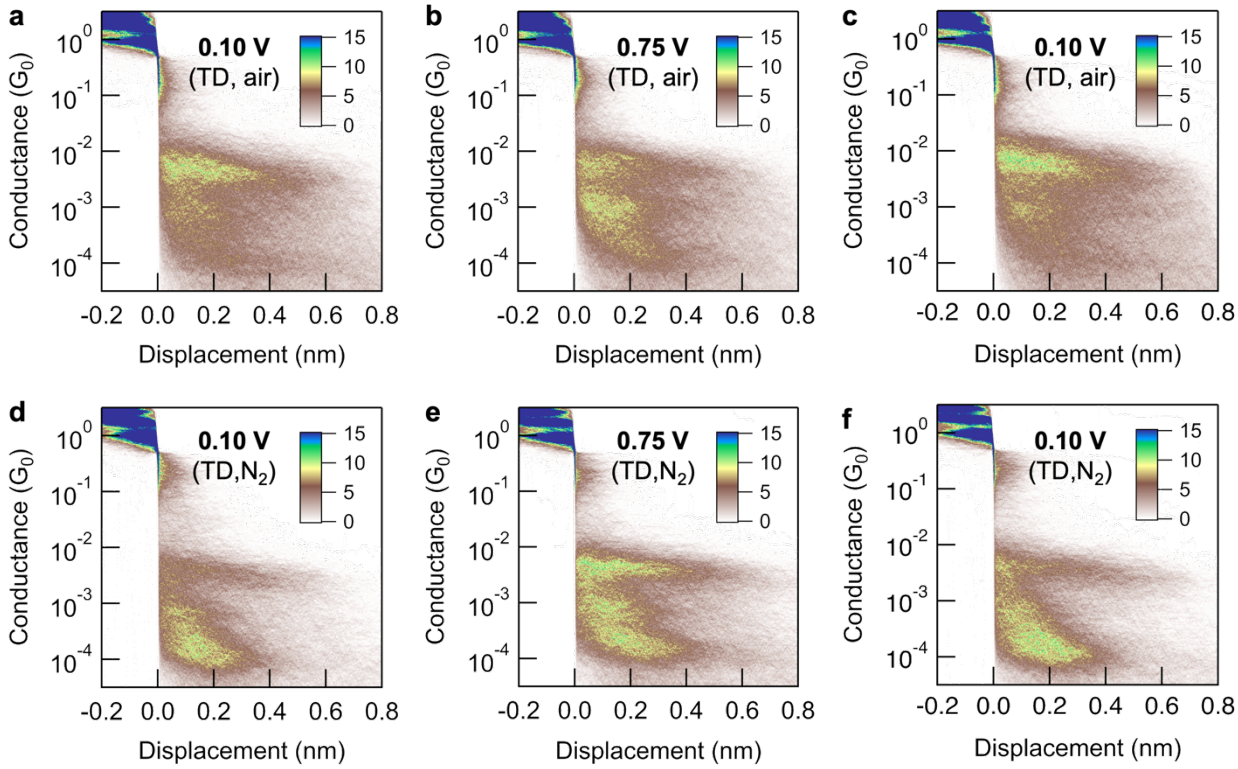

Figure S5. 2D conductance-displacement histograms obtained from measurements of **ᵗBu**, corresponding to the 1D conductance histograms shown in **Figure 3a,b**.

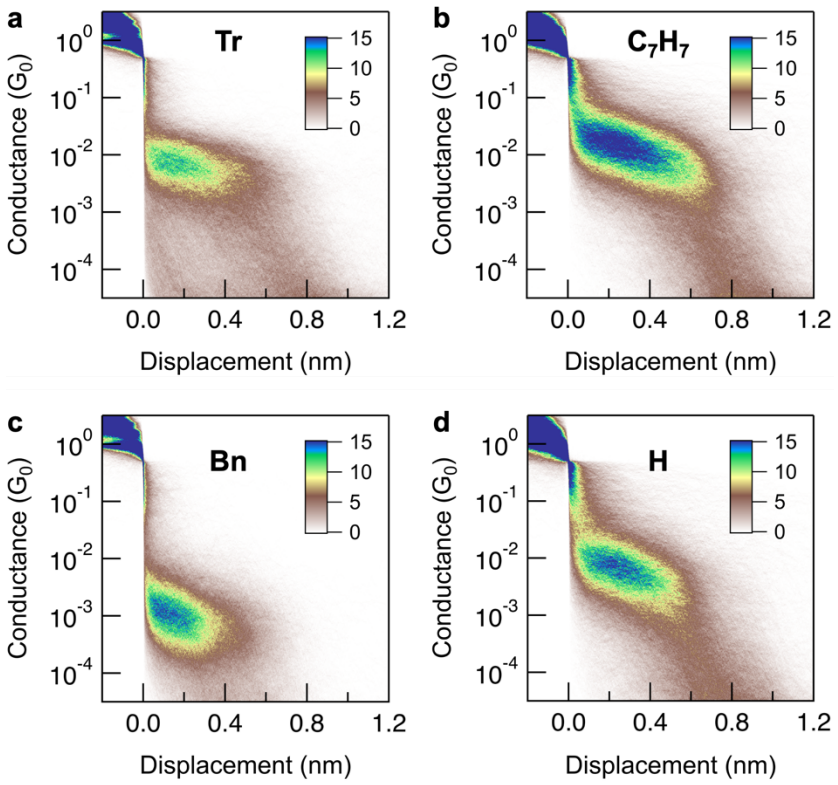

Figure S6. 2D conductance-displacement histograms corresponding to the 1D conductance histograms shown in **Figure 4a** for **(a) Tr**, **(b) C_7H_7**, **(c) Bn**, **(d) H** (reproduced here from a previous report,[1] for convenience).

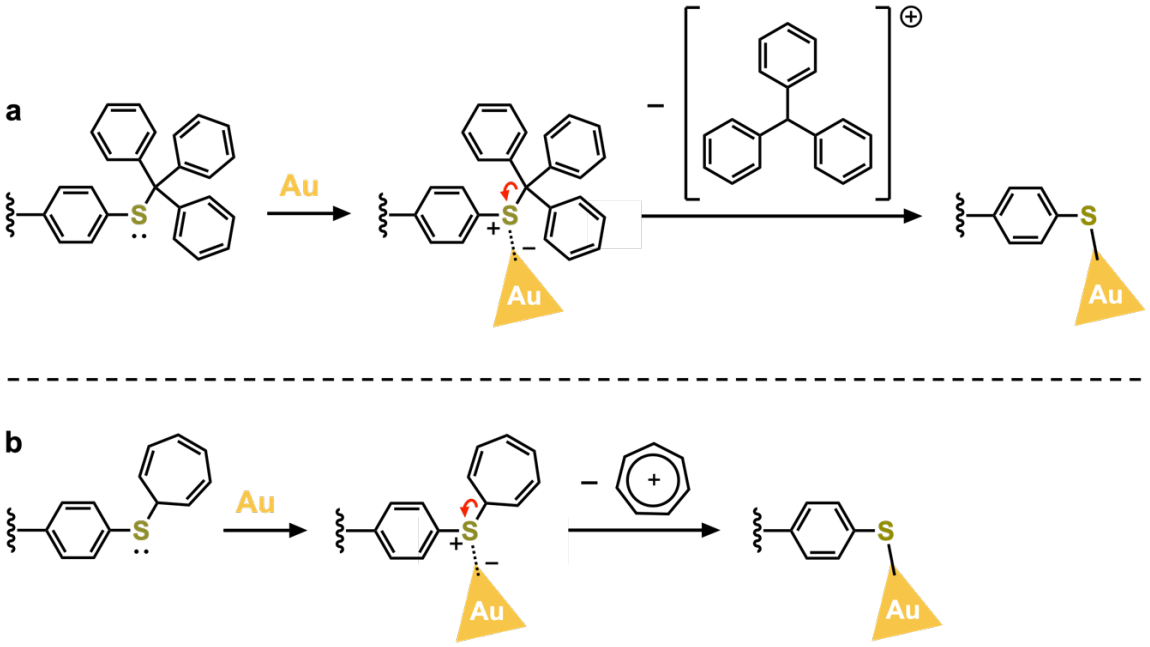

Figure S7. Proposed reaction mechanisms for the *in situ* cleavage of **(a)** tritylium ($[CPh_3]^+$) and **(b)** tropylium ($[C_7H_7]^+$) carbocations upon coordination of a Lewis basic sulfur group to a Lewis acidic undercoordinated gold adatom.

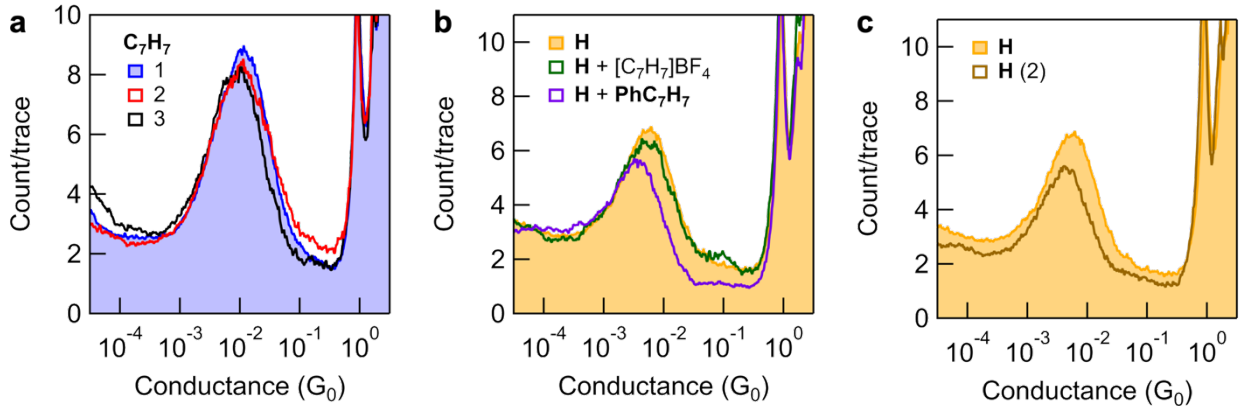

Figure S8. (a) Overlaid 1D histograms for repeated measurements of **C_7H_7** (5,000-10,000 traces, V_{bias} = 0.10 V), with solution concentrations varied between 0.1-1 mM. This data shows that junctions formed from **C_7H_7** consistently exhibit a higher conductance than those formed from **H**. The filled histogram for **C_7H_7** (1) is reproduced here from **Figure 4a** for convenience. **(b)** Overlaid 1D histograms obtained from measurements of 0.1-0.2 mM solutions of **H** in the presence of two molar equivalents of $[C_7H_7]BF_4$ or **PhC_7H_7** (5,000-10,000 traces, V_{bias} = 0.10 V). These control studies show that the presence of $[C_7H_7]^+$ – either in bulk solution or generated at the gold surface following coordination of **PhC_7H_7** – does not influence the peak intensity or conductance for junctions formed from **H**. **(c)** Overlaid 1D histograms for repeated measurements of **H**, showing experiment to experiment variation. This indicates the small shift to lower conductance, and reduced intensity of the peak in the "**H** + **PhC_7H_7**" histogram in panel (b) is not necessarily attributable to the presence of **PhC_7H_7**. Filled histograms for **H** in panels (b), (c) are reproduced here from a previous report[1] for convenience.

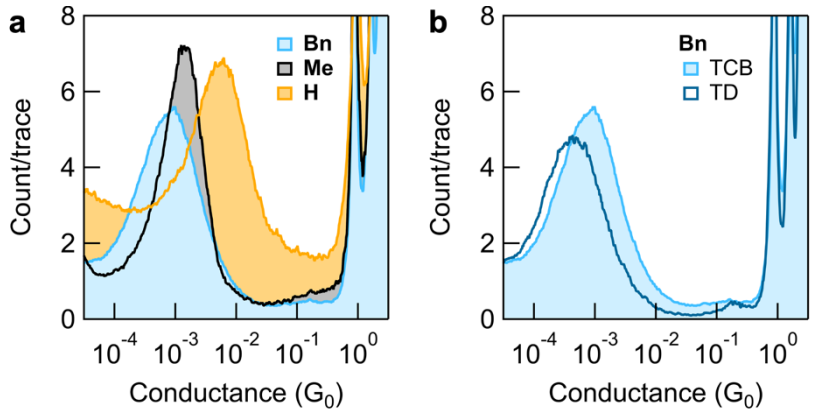

Figure S9. (a) Overlaid 1D conductance histograms obtained from measurements of **(a) Bn**, **Me**, and **H** in TCB and **(b) Bn** in TCB and TD (5,000-10,000 traces, V_{bias} = 0.10 mV). The lower conductance of **Bn** junctions relative to those formed from **Me** or **H**, even in TD, provides strong evidence that the thioether group remains intact during STM-BJ studies; these junctions exhibit a PP geometry, $[PhCH_2]^+$ is not cleaved. The filled histogram for **Bn** measurements is reproduced from **Figure 4a**, and data for **Me** and **H** is reproduced from a previous report,[1] for convenience.

4. Additional Computational Data

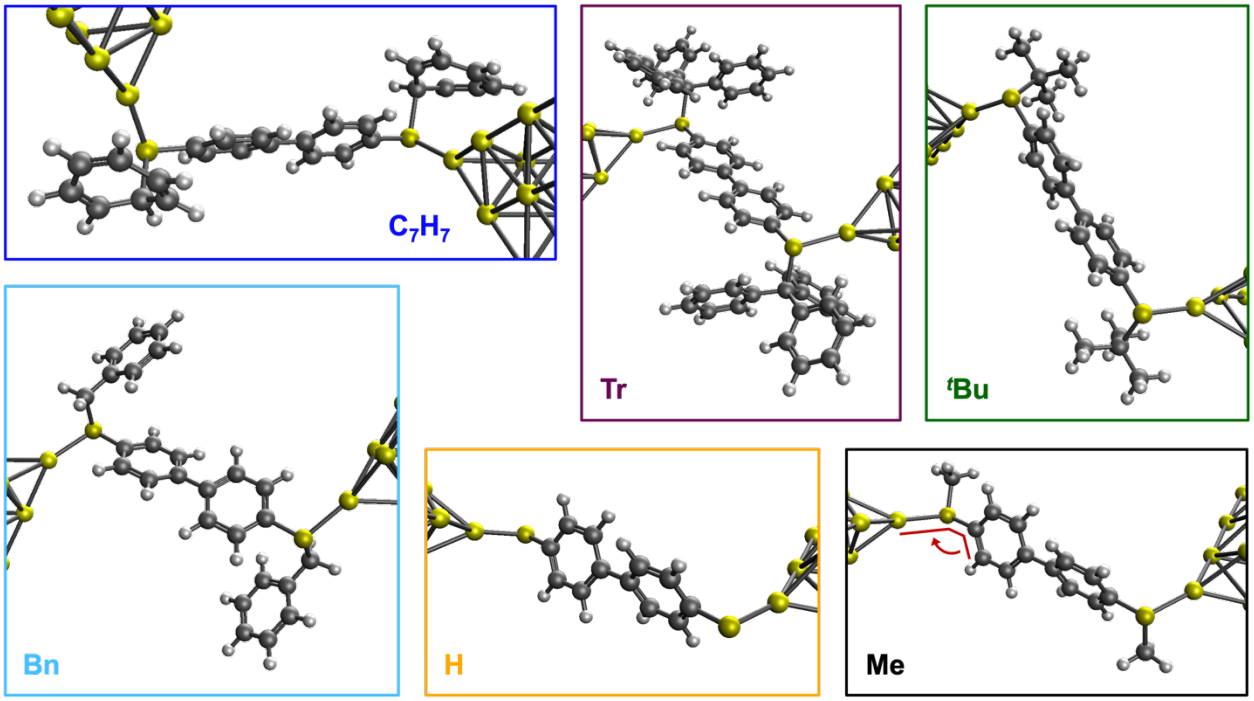

Figure S10. Optimized geometries of **C_7H_7**, **^{t}Bu**, **Bn**, **H**, and **Me** junctions. For **Tr** junctions, the full geometry of **Tr** is frozen in relaxed configuration obtained for the complex after addition of single gold atoms to each sulfur atom. We found that relaxation of the **Tr** junction after addition of extended gold electrodes resulted in spontaneous S-C bond cleavage to form the tritylium cation. Note that all junctions comprise physisorbed Au-S(R) linkages except for **H** which exhibits a chemisorbed S-Au contact, in line with expectations for solution measurements of thiol-functionalized molecules.[5] The Au-S-C-C dihedral angle is defined for **Me** (red lines), and is calculated for each junction, along with additional structural parameters, in **Table S4**.

Table S4. Selected structural parameters for optimized junction geometries.[a]

junction	dihedral angles (°) [b]	avr. deviation from 90 (°) [b]	Au-S (Å)	S-C (Å) [c]
C_7H_7	130.41, 128.14	39.28	2.3680, 2.3709	2.0765, 2.0269
Tr [d]	153.83, 153.83	63.83	2.5060, 2.5060	1.9947, 1.9947
^{t}Bu	141.71, 144.46	53.09	2.4119, 2.4028	1.9031, 1.9048
Bn	143.77, 161.044	62.41	2.4156, 2.4072	1.8702, 1.8765
H	95.73, 81.59	7.07	2.3039, 2.3051	-
Me	98.09, 88.39	4.85	2.4409, 2.4458	1.8208, 1.8183

[a] See **Figure S10** for junction geometries and further discussion. [b] Absolute angles are reported. A dihedral of 90° is close to the optimal value for electronic coupling between the Au-S bind and the conjugated π-orbitals of the backbone.[18] [c] The carbon atom of the thioether substituent, i.e., the methyl group of **Me**. [d] The geometry of **Tr** junctions was not fully optimized (see **Figure S10**).

Table S5. Additional computational data for biphenyl-based molecules and junction models.[a]

molecule	HOMO-LUMO gap (eV) [b]	calculated conductance (G_0) [c]
C_7H_7	2.622	1.02×10^{-4}
Tr [d]	2.751	3.35×10^{-5}
^{t}Bu	2.941	1.85×10^{-4}
Bn	2.831	1.54×10^{-4}
H	3.141	7.13×10^{-2}
Me	3.022	9.60×10^{-3}

[a] See *Computational Details* section for more information on the methods used. [b] For the gas phase molecule before adding gold electrodes/clusters. [c] The transmission at E_F, obtained from the DFT-NEGF calculations presented in **Figure 4c**.

5. NMR Spectra

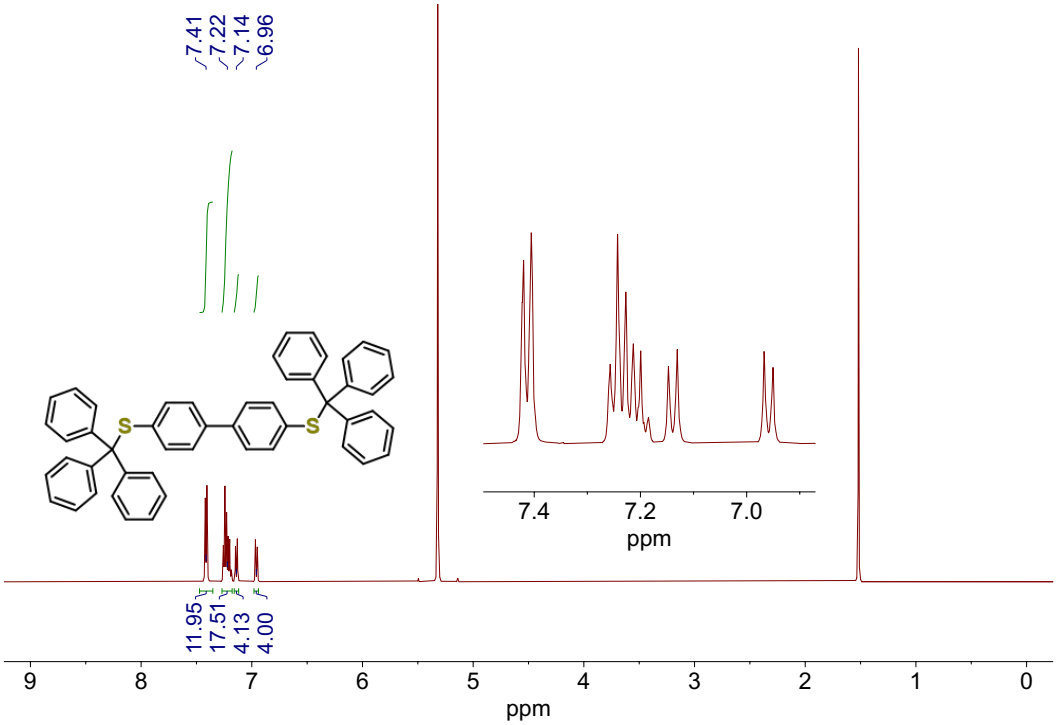

Figure S11. ^{1}H NMR (500 MHz) spectrum of **Tr** in CD_2Cl_2.

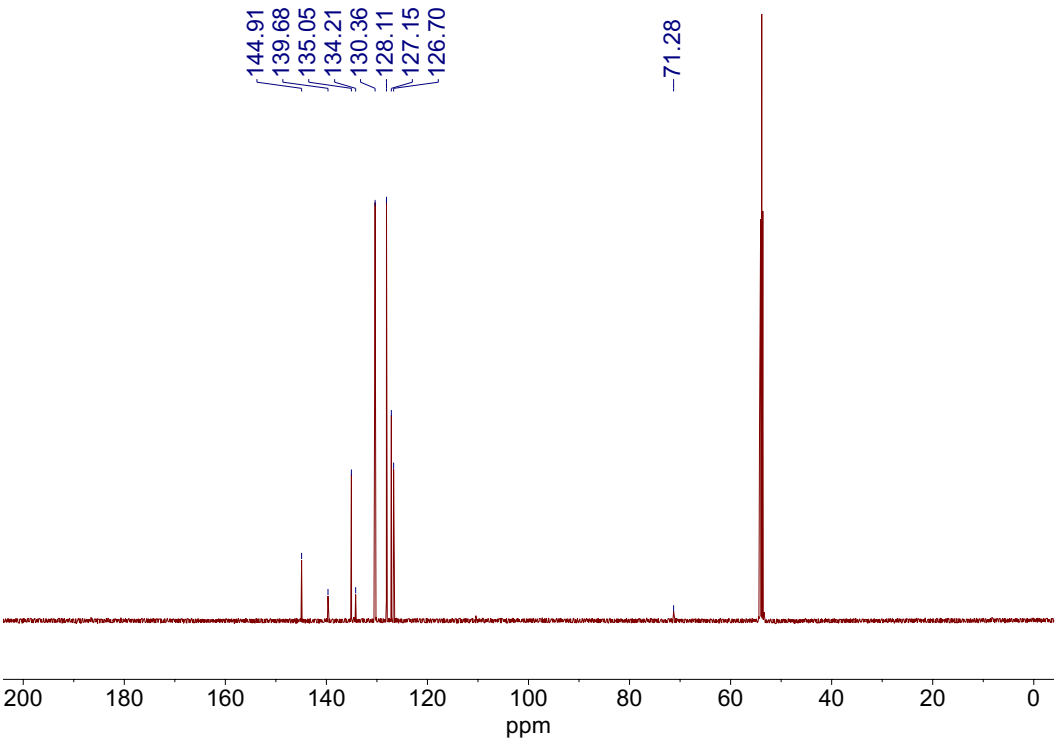

Figure S12. ^{13}C{^{1}H} NMR (126 MHz) spectrum of **Tr** in CD_2Cl_2.

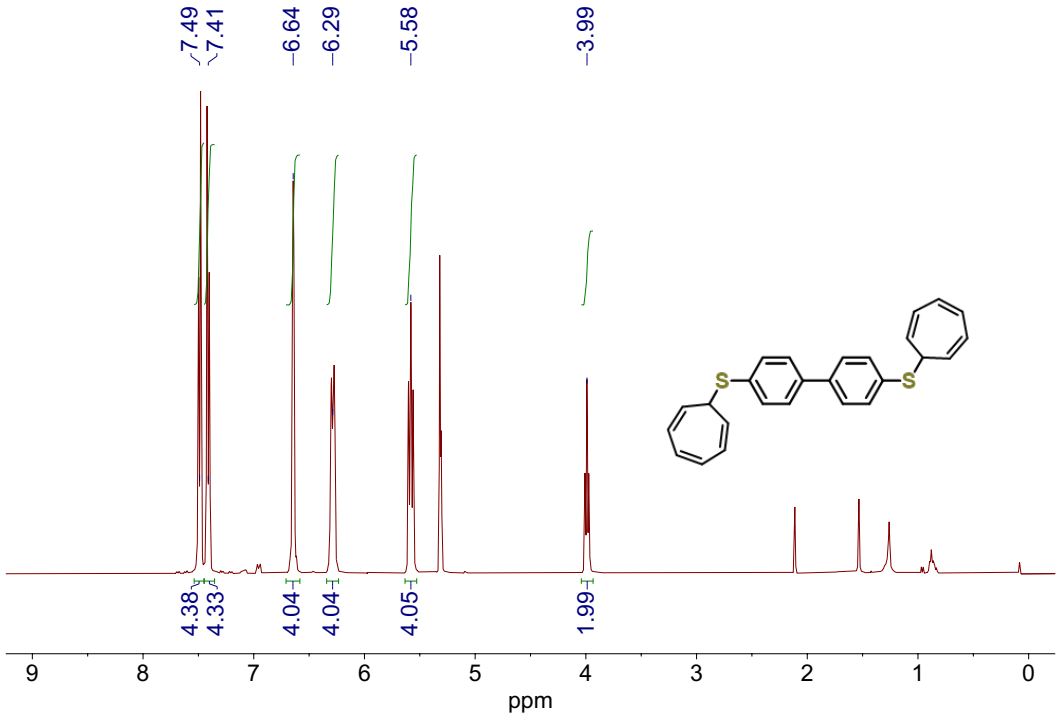

Figure S13. ^{1}H NMR (400 MHz) spectrum of $\mathbf{C_7H_7}$ in CD_2Cl_2.

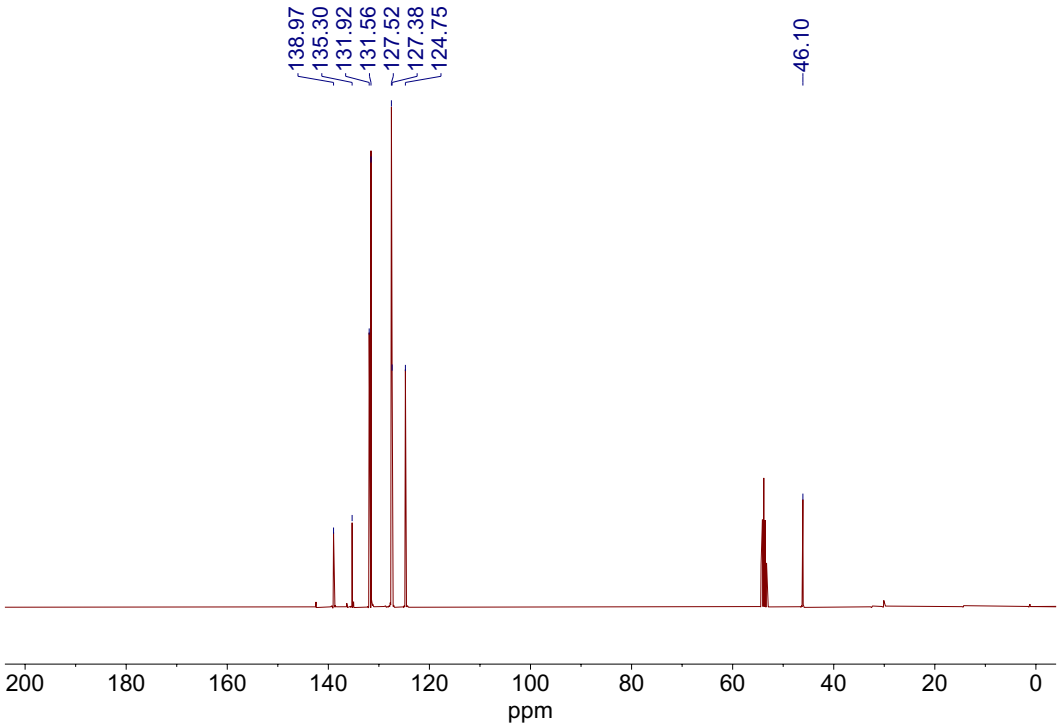

Figure S14. ^{13}C{^{1}H} NMR (101 MHz) spectrum of $\mathbf{C_7H_7}$ in CD_2Cl_2.

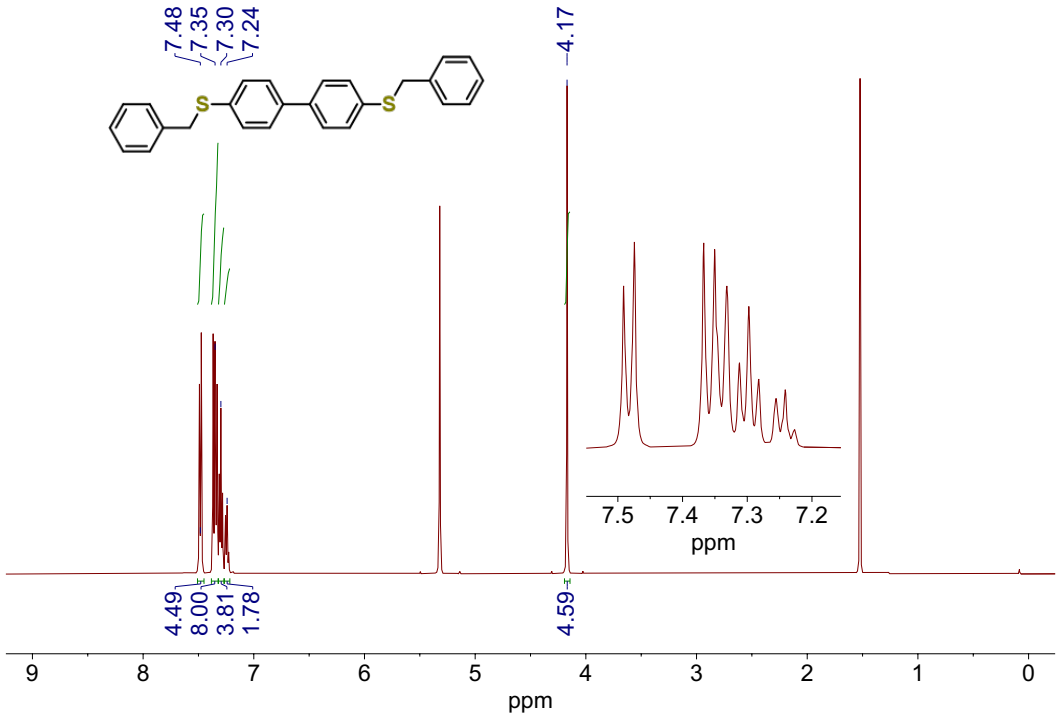

Figure S15. ^{1}H NMR (500 MHz) spectrum of **Bn** in CD_2Cl_2.

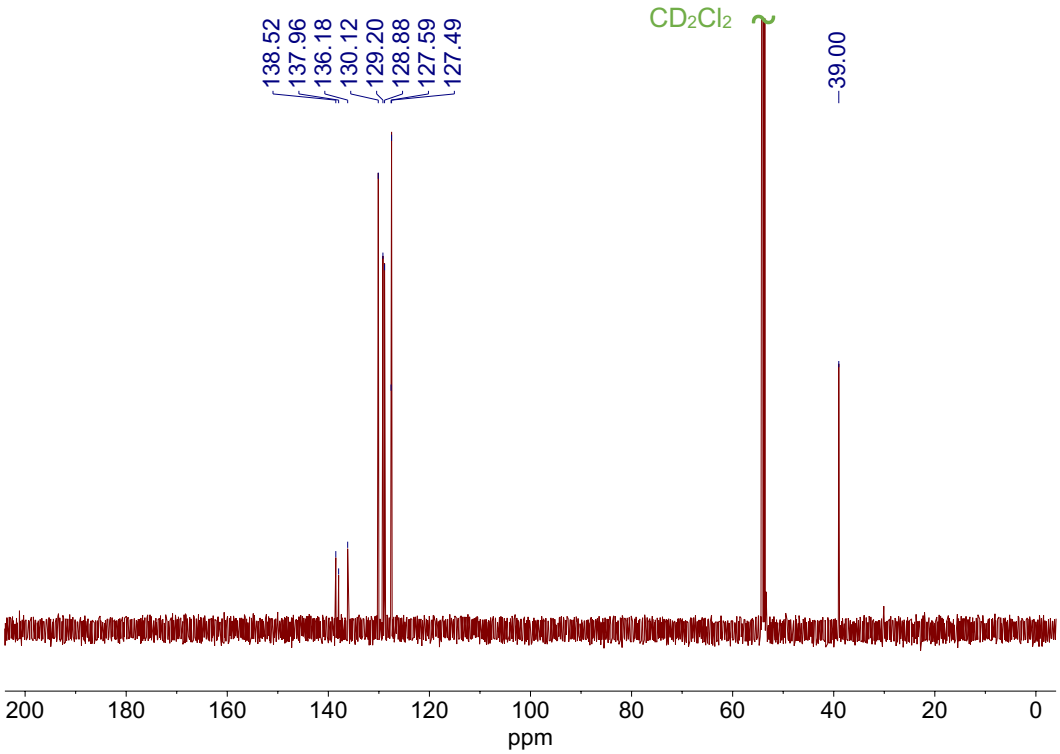

Figure S16. ^{13}C{^{1}H} NMR (126 MHz) spectrum of **Bn** in CD_2Cl_2.

6. References

(1) Prana, J.; Kim, L.; Czyszczon-Burton, T.; Homann, G.; Chen, S.; Miao, Z.; Camarasa-Gomez, M.; Inkpen, M. Lewis-Acid Mediated Reactivity in Single-Molecule Junctions. *J. Am. Chem. Soc.* **2024**, *146* (48), 33265–33275.

(2) Fulmer, G. R.; Miller, A. J. M.; Sherden, N. H.; Gottlieb, H. E.; Nudelman, A.; Stoltz, B. M.; Bercaw, J. E.; Goldberg, K. I. NMR Chemical Shifts of Trace Impurities: Common Laboratory Solvents, Organics, and Gases in Deuterated Solvents Relevant to the Organometallic Chemist. *Organometallics* **2010**, *29* (9), 2176–2179.

(3) Kim, L.; Czyszczon-Burton, T. M.; Nguyen, K. M.; Stukey, S.; Lazar, S.; Prana, J.; Miao, Z.; Park, S.; Chen, S. F.; Inkpen, M. S. Low Vapor Pressure Solvents for Single-Molecule Junction Measurements. *Nano Lett.* **2024**, *24* (32), 9998–10005.

(4) Venkataraman, L.; Klare, J. E.; Tam, I. W.; Nuckolls, C.; Hybertsen, M. S.; Steigerwald, M. L. Single-Molecule Circuits with Well-Defined Molecular Conductance. *Nano Lett.* **2006**, *6* (3), 458–462.

(5) Inkpen, M. S.; Liu, Z.; Li, H.; Campos, L. M.; Neaton, J. B.; Venkataraman, L. Non-Chemisorbed Gold–Sulfur Binding Prevails in Self-Assembled Monolayers. *Nature Chem.* **2019**, *11*, 351–358.

(6) Miao, Z.; Quainoo, T.; Czyszczon-Burton, T. M.; Rotthowe, N.; Parr, J. M.; Liu, Z.; Inkpen, M. S. Charge Transport across Dynamic Covalent Chemical Bridges. *Nano Lett.* **2022**, *22* (20), 8331–8338.

(7) Nagahara, L. A.; Thundat, T.; Lindsay, S. M. Preparation and Characterization of STM Tips for Electrochemical Studies. *Rev. Sci. Instr.* **1989**, *60* (10), 3128–3130.

(8) Williams, D. B. G.; Lawton, M. Drying of Organic Solvents: Quantitative Evaluation of the Efficiency of Several Desiccants. *J. Org. Chem.* **2010**, *75* (24), 8351–8354.

(9) Blum, V.; Gehrke, R.; Hanke, F.; Havu, P.; Havu, V.; Ren, X.; Reuter, K.; Scheffler, M. Ab Initio Molecular Simulations with Numeric Atom-Centered Orbitals. *Comp. Phys. Commun.* **2009**, *180* (11), 2175–2196.

(10) Perdew, J. P.; Burke, K.; Ernzerhof, M. Generalized Gradient Approximation Made Simple. *Phys. Rev. Lett.* **1996**, *77* (18), 3865–3868.

(11) Lenthe, E. V.; Baerends, E. J.; Snijders, J. G. Relativistic Regular Two-Component Hamiltonians. *J. Chem. Phys.* **1993**, *99* (6), 4597–4610.

(12) Camarasa-Gómez, M.; Hernangómez-Pérez, D.; Evers, F. Spin–Orbit Torque in Single-Molecule Junctions from Ab Initio. *J. Phys. Chem. Lett.* **2024**, *15* (21), 5747–5753.

(13) Arnold, A.; Weigend, F.; Evers, F. Quantum Chemistry Calculations for Molecules Coupled to Reservoirs: Formalism, Implementation, and Application to Benzenedithiol. *J. Chem. Phys.* **2007**, *126* (17), 174101.

(14) Bagrets, A. Spin-Polarized Electron Transport Across Metal–Organic Molecules: A Density Functional Theory Approach. *J. Chem. Theory Comput.* **2013**, *9* (6), 2801–2815.

(15) Lichte, D.; Pirkl, N.; Heinrich, G.; Dutta, S.; Goebel, J. F.; Koley, D.; Gooßen, L. J. Palladium-Catalyzed Para-C−H Arylation of Anilines with Aromatic Halides. *Angew. Chem. Int. Ed.* **2022**, *61* (47).

(16) Cavazza, M.; Morganti, G.; Pietra, F. Synthesis of (7-(Alkylthio)- and 7-(Arylthio)Cycloheptatriene)Tricarbonyliron and -Hexacarbonyldiiron Complexes. *J. Org. Chem.* **1980**, *45* (10), 2001–2004.

(17) Kobayashi, K.; Koyama, E.; Kono, C.; Namatame, K.; Nakamura, K.; Furukawa, N. Evidence for Intermolecular Interaction between Sulfonium and Sulfide Sulfur Atoms and Its Application to Synthesis of Cyclic Bis(Disulfide) Dimer. *J. Org. Chem.* **2001**, *66* (6), 2085–2090.
(18) Park, Y. S.; Widawsky, J. R.; Kamenetska, M.; Steigerwald, M. L.; Hybertsen, M. S.; Nuckolls, C.; Venkataraman, L. Frustrated Rotations in Single-Molecule Junctions. *J. Am. Chem. Soc.* **2009**, *131* (31), 10820–10821.